IEEE Access
Multidisciplinary | Rapid Review | Open Access Journal

Received February 18, 2021, accepted March 21, 2021, date of publication March 29, 2021, date of current version April 6, 2021.

Digital Object Identifier 10.1109/ACCESS.2021.3069281

Simulation of Optimized High-Current Tandem Solar-Cells With Efficiency Beyond 41%

MOHAMED MOUSA[1], FATHY Z. AMER[2], ROAA I. MUBARAK[2], AND AHMED SAEED[1], (Senior Member, IEEE)

[1]Electrical Engineering Department, Future University in Egypt, Cairo 11835, Egypt
[2]Department of Electronics and Communications Engineering, Faculty of Engineering, Helwan University, Cairo 11792, Egypt

Corresponding author: Mohamed Mousa (mohamed.mossa@fue.edu.eg)

ABSTRACT Two-terminal tandem solar-cells have a high efficiency of power conversion. One of their main limitations is the operating current density as the two-terminal tandem solar-cell is equivalent to electrically connected series subcells. Increasing the top absorber layer's thickness will lead to an increase in the top subcell current and a decrease in the bottom subcell's current. The subcell with the minimum current forces the tandem cell to operate at its value, limiting the overall performance. In this paper, a proposed solution for such a problem is introduced using a bottom subcell consisting of germanium-telluride (GeTe), which gives a high current and matches the top subcell at a thicker absorber layer. A proposal of three different tandem cells with perovskite ($MAPbI_3$)/CIGS, perovskite ($MAPbI_3$)/GeTe, and perovskite ($MAPbI_{3-x}Cl_x$)/GeTe have been presented. The proposed perovskite ($MAPbI_3$)/CIGS has an efficiency of 30.52%, whereas the replacement of the CIGS bottom subcell by GeTe led to a significant enhancement of the efficiency to reach 35.9%. High efficiency of 41.7% is obtained by replacing the perovskite ($MAPbI_3$) top subcell with perovskite ($MAPbI_{3-x}Cl_x$). A modified numerical algorithm is proposed to obtain the optimum thickness of the top subcell to achieve higher power-conversion efficiency. The performance evaluation and simulation of the designed tandem cells were carried out using SCAPS-1D. The temperature effects on the proposed cells have been encountered in simulation. The results show that the proposed tandem solar-cells have comparable performance and higher efficiencies relative to the published works.

INDEX TERMS CIGS, GeTe, high-current tandem-cell, optimized thickness, perovskite, two-terminal tandem-solar cell, SCAPS-1D.

I. INTRODUCTION

The demand for energy has risen dramatically in the last century. In the next few decades, it is expected that this demand will be doubled. The main source of the used energy now is fossil fuels, which has a terrible impact on the environment and leads to global warming. Clean energy devices are promising for the commercial market, especially photovoltaics, due to their advantages of providing clean energy, converting sunlight into electricity without pollution, and operating for a long time without maintenance [1].

Nowadays, the different forms of crystalline silicon (Si) solar cells dominate the market of photovoltaic. More than 25 % efficiency can be achieved by the silicon solar cells [2]. Copper indium gallium selenide (CIGS) is considered to be one of the most promising and efficient thin-film solar cells with a thin window layer of tungsten disulfide (WS_2) to have a simulated efficiency of about 26.4% [3], also perovskite solar cells have demonstrated fast development and opened new ways for photovoltaic as it is reported efficiency has increased in the recent few years up to more than 30% [4]. The reasons behind the increase of perovskite cells' performance are their lower recombination rates, broad absorb spectrum, long diffusion lengths, high open-circuit voltage, and bandwidth tuning.

The performance of this type of solar cells is limited as it can only absorb the photons with the energies greater than or equal to the energy gap of the used material, while the other part of the incident spectrum will be lost, and even

The associate editor coordinating the review of this manuscript and approving it for publication was Z. G. Zang.

photons with higher energies will lose the energy difference as a thermalization loss.

This limit can be overcome by the promising tandem (multi-junction) photovoltaic devices as they consist of sub-cells, each of which absorbs different wavelengths of the incident spectrum [5].

In this work, three different proposed tandem solar cells are tested and simulated at different conditions using SCAPS-1D (SC Capacitance Simulator-one dimension) [6]. High efficiency of 30.5% is obtained using ($MAPbI_3$)/CIGS tandem cell.

The replacement of the CIGS bottom subcell by GeTe subcell with the same doping level and thickness has solved the current limiting problem, which improved the efficiency to reach 35.9%. Then, the perovskite ($MAPbI_3$) top subcell is replaced with the perovskite ($MAPbI_{3-x}Cl_x$) subcell, which has higher performance parameters, as the mixed iodide/chloride perovskite have higher thermal stability and better carrier diffusion lengths, which led to a very high efficiency of about 41.7%.

In addition, the performance of the three tandem cells are tested at different temperatures, and the results show that the tandem cells with GeTe as a bottom subcell is more immune to temperature variations than the tandem cell with the CIGS as a bottom subcell.

The rest of this work is structured as follows: the methodology is discussed in section II; section III presents the simulation results and discussion; section IV shows the effects of the temperature on the performance parameters; a comparison of the results of this work and the recently published results are presented in section V; finally, section VI provides the concluding remarks.

II. METHODOLOGY

A. CELL STRUCTURE

Through the investigation of the performance of the tandem solar cells, the top and bottom subcells are simulated independently. Following the widely used approach in simulating the tandem cells, it is assumed that the tunnel junction is ideal, and the electrical losses and optical losses in each interface are neglected [7]–[12].

The current matching condition is achieved by adjusting the thickness of the top subcell while fixing the thickness of the bottom subcell. The structure of perovskite ($MAPbI_3$), perovskite ($MAPbI_{3-x}Cl_x$) top subcells and CIGS, and GeTe bottom subcells are shown in Fig. 1.

In the perovskite ($MAPbI_3$) subcell, copper oxide (Cu_2O) is used as a Hole Transport Layer (HTL), PCBM (fullerene derivative of the C_{60} buckyball) is used as an Electron Transport Layer (ETL), and the $MAPbI_3$ as an active layer.

In the perovskite ($MAPbI_{3-x}Cl_x$) subcell, the CuO is used as HTL, the ZnOS is used as ETL, and the $MAPbI_{3-x}Cl_x$ is the active layer. Transparent Conductive Oxides (TCO) and two Interface defect layers (IDLs) are used. The TCO operates as an optically-transparent electrode that allows photons

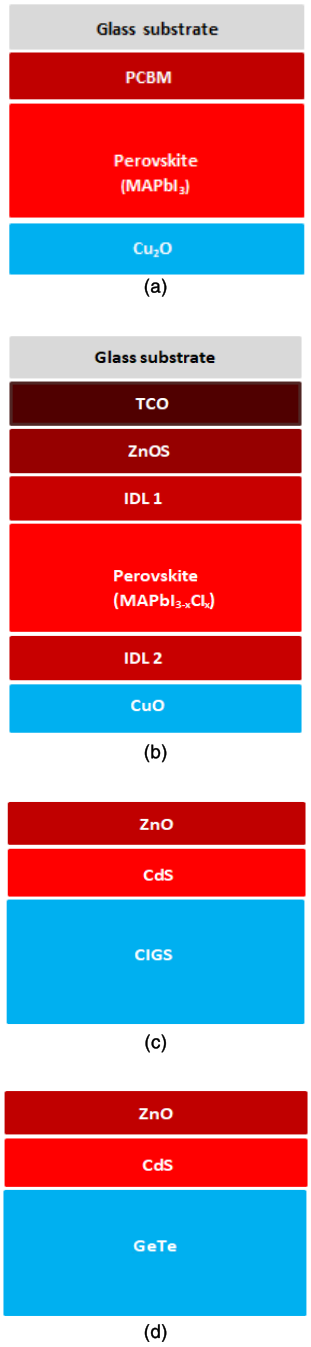

FIGURE 1. Cross section of (a) perovskite ($MAPbI_3$), (b) perovskite ($MAPbI_{3-x}Cl_x$), (c) CIGS, and (d) GeTe subcells.

to penetrate the cell and carry the generated electrons to the external terminals of the cell. In contrast, the IDLs are used between the active layer ($MAPbI_{3-x}Cl_x$) and the HTL layer, and between the active layer ($MAPbI_{3-x}Cl_x$) and the ETL layer to make the device more practical. In the CIGS and GeTe subcells, zinc oxide (ZnO) and Cadmium sulfide (CdS) are used before the absorption layer.

The simulation parameters of the top and bottom subcells are based on the models used in [4], [7], and [13], which are listed in Tables 1, 2, and 3.

TABLE 1. Simulation parameters of perovskite ($MAPbI_3$) top subcell.

Parameters	Cu_2O	$MAPbI_3$	PCBM
E_g (eV)	2.45 [15]	1.50 [16]	1.80 [17]
Thickness (nm)	20	(variable)	25
Relative permittivity	7.11 [18]	6.50 [19]	3.90 [19]
Affinity of the electrons (eV)	2.6	3.9	4.2
Effective density of states of CB (cm^{-3})	2.02×10^{17} [18]	2.75×10^{18} [20]	10^{21} [21]
Mobility of the electrons μ_e ($cm^{-2}V^{-1}s^{-1}$)	200 [22]	10 [23]	10^{-3} [19]
Concentration of donors N_D (cm^{-3})	0	10^{13} [24]	10^{18}
Effective density of states of VB (cm^{-3})	1.1×10^{19} [18]	3.9×10^{18} [20]	10^{21} [21]
Mobility of the holes μ_p ($cm^{-2}V^{-1}s^{-1}$)	80 [25]	10 [23]	2×10^{-3} [19]
Concentration of acceptors N_A (cm^{-3})	10^{18} [26]	10^{13} [24]	0
Density of defects N_t (cm^{-3})	10^{14}	10^{14}	10^{14}

TABLE 2. Simulation parameters of perovskite ($MAPbI_{3-x}Cl_x$) top subcell.

Parameters	*CuO*	*IDL*	*$MAPbI_{3-x}Cl_x$*	*ZnOS*	*TCO*
E_g (eV)	2.1 [27]	1.55	1.5 [28]	2.83[29]	3.5
Thickness(nm)	300	10	(variable)	20	500
Relative permittivity	7.11 [27]	6.5	6.5 [27]	9 [29]	9
Affinity of electrons(eV)	3.2 [27]	3.9	3.9 [30]	3.6 [31]	4
Effective density of states of CB (cm^{-3})	2.2×10^{18}	2.2×10^{18}	2.2×10^{18}	2.2×10^{18}	2.2×10^{18}
Mobility of the electrons μ_e ($cm^{-2}V^{-1}s^{-1}$)	3.4	2	2 [27]	100 [29]	20
Concentration of donors N_D (cm^{-3})	0	10^{15}	10^{13} [4]	10^{18} [4]	2×10^{19}
Effective density of states of VB (cm^{-3})	1.8×10^{18}	1.8×10^{18}	1.8×10^{18}	1.8×10^{19}	1.8×10^{18}
Mobility of the holes μ_p ($cm^{-2}V^{-1}s^{-1}$)	3.4	2	2 [27]	25 [29]	10
Concentration of acceptors N_A (cm^{-3})	10^{20}	0	0	0	0
Density of defects N_t (cm^{-3})	10^{15}	10^{15}	10^{10} [32]	10^{15}[33]	10^{15}[33]

The power density of the light spectrum transmitted from the top subcell to the bottom subcell, $S(\lambda)$ (W/m^2), is given by (1) [8];

$$S(\lambda) = S_o(\lambda) \cdot \prod_{x=1}^{n} e^{-\alpha_x d_x} \quad (1)$$

where S_o is the incident spectrum (AM 1.5), x is the layer number, n is the total number of layers of the subcell, d is the thickness of each layer (cm), and α is the absorption coefficient (cm^{-1}) of each material (with a pre-factor A_α) given by [14];

$$\alpha(E) = A_\alpha \sqrt{h\nu - E_g} \quad (2)$$

where E_g is the energy gap of the material (eV), h is the Plancks constant (eV.sec), and ν is the spectrum frequency.

TABLE 3. Simulation parameters of bottom CIGS and GeTe subcells.

Parameters	GeTe	CIGS	CdS	ZnO
E_g (eV)	0.8 [13]	1.10[34]	2.45[35]	3.30[35]
Thickness (nm)	2000	2000	50	20
Relative permittivity	36 [13]	13.6 [7]	10.0 [7]	9.0 [7]
Affinity of the electrons (eV)	4.8	4.5	4.4	4.6
Effective density of states of CB (cm^{-3})	10^{16}	2.2×10^{18}	2.2×10^{18}	2.2×10^{18}
Mobility of the electrons μ_e ($cm^{-2}V^{-1}s^{-1}$)	100	100	100	100
Concentration of donors N_D (cm^{-3})	0	0	10^{20}	10^{20}
Effective density of states of VB (cm^{-3})	10^{17}	1.8×10^{19}	1.8×10^{19}	1.8×10^{19}
Mobility of the holes μ_p ($cm^{-2}V^{-1}s^{-1}$)	20	25	25	25
Concentration of acceptors N_A (cm^{-3})	2×10^{16}	2×10^{16}	0	0
Density of defects N_t (cm^{-3})	10^{14}	10^{14}	10^{14}	10^{14}

B. THICKNESS OPTIMIZATION OF THE TOP SUBCELL

In this subsection, a modified numerical method based on the concept given by [36] is proposed. The proposed modification in the algorithm uses two phases for thickness (t_s) optimization with two steps: course step t_{cs} of 50 nm, and fine step t_{fs} of 5 nm. The flowchart of the proposed algorithm is shown in Fig. 2. In each step, all the performance parameters of the junction is calculated based on the resulting thickness.

This proposed change leads to faster response in finding the optimum top subcell thickness for the two junction tandem cell, as the number of total calculations decreases. Moreover, it can find more accurate optimum thickness as the step of the second phase is reduced to 5 nm. The bottom subcell layer thickness must be thick to absorb as much as possible from the transport photons from the top subcell and was not taken into considerations in the optimization process, but the overall thickness of the tandem structure must not be greater than 50 μm (an assumed diffusion length to ensure free charge transport to electrodes) [36].

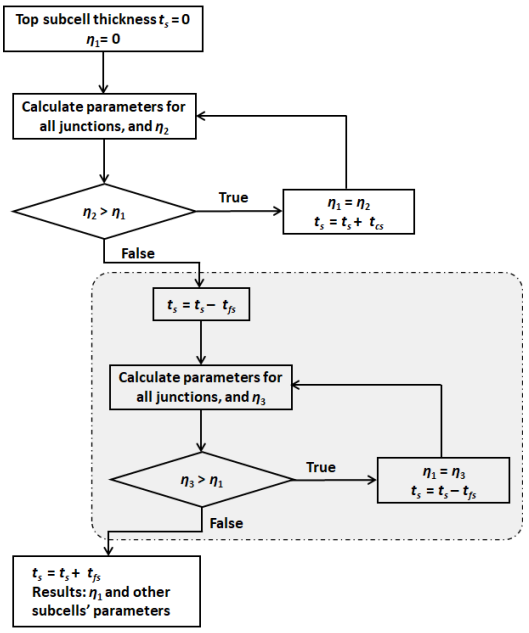

FIGURE 2. Flowchart of optimization technique of top subcell thickness for two junction tandem solar cells.

III. SIMULATION RESULTS AND DISCUSSION

A. PEROVSKITE ($MAPbI_3$) SUBCELL

In this section, the study of simulating perovskite ($MAPbI_3$) subcell is performed. The Cu_2O layer valence band maximum is −5.05 eV, i.e., higher than the Highest Occupied Molecular Orbital (HOMO) energy level of the $MAPbI_3$layer (−5.5 eV), thus leading to the extraction of the holes at the interface between $MAPbI_3$ and Cu_2O layers. Furthermore, the edge of conduction of the Cu_2O film is (−2.60 eV), which is much higher than the Lowest Unoccupied Molecular Orbital (LUMO) level of the $MAPbI_3$ (−3.9 eV). This blocks electrons from $MAPbI_3$ to reach the Cu_2O layer effectively. On the other side, the HOMO level of the PCBM layer is lower than that of the $MAPbI_3$ layer, and PCBM shows a slightly deeper LUMO level than $MAPbI_3$. This causes the holes and electrons to be successfully drifted to the contacts. The perovskite ($MAPbI_3$) subcell performance is studied for different active layer ($MAPbI_3$) thickness range of 50 nm to 600 nm. The variation of Power Conversion Efficiency (*PCE*), open-circuit voltage (V_{OC}), short-circuit current density (J_{SC}), and Fill Factor (*FF*) with $MAPbI_3$ thickness variations are shown in Fig. 3.

B. PEROVSKITE ($MAPbI_{3-x}Cl_x$) SUBCELL

In this section, the study of simulating perovskite ($MAPbI_{3-x}Cl_x$) subcell is performed. The variations of *PCE*, V_{OC}, J_{SC}, and *FF* with ($MAPbI_{3-x}Cl_x$) thickness are shown in Fig. 4. The perovskite ($MAPbI_{3-x}Cl_x$) subcell is more complicated than the perovskite ($MAPbI_3$) subcell; however, the simulation results show higher *PCE*, J_{SC}, and *FF* at any absorber layer thickness. On the other hand, the V_{OC} of perovskite ($MAPbI_{3-x}Cl_x$) is lower than perovskite ($MAPbI_3$) at a small layer thickness. However, unlike

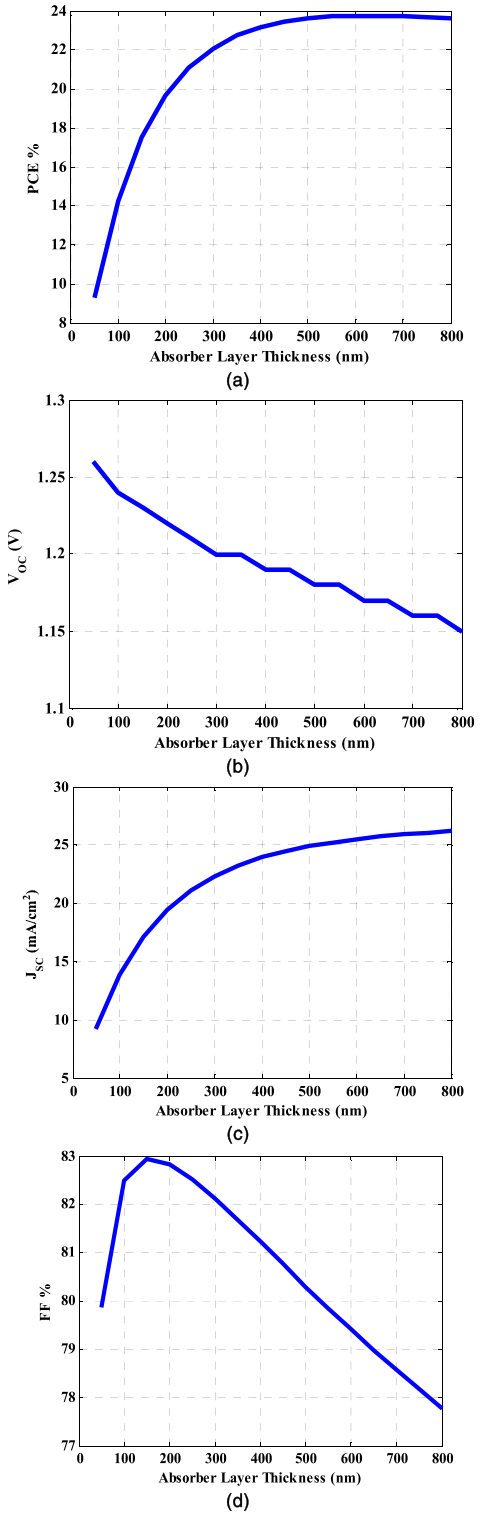

FIGURE 3. Characteristics of perovskite ($MAPbI_3$) with absorber thickness (*T* is 300 K, AM 1.5; electron and hole thermal velocities of 10^7 (cm/s)): (a) *PCE*, (b) V_{OC}, (c) J_{SC}, and (d) *FF*.

the perovskite ($MAPbI_3$) subcell, the V_{OC} of the perovskite ($MAPbI_{3-x}Cl_x$) subcell does not decrease by increasing the absorber layer thickness; instead, it increases until reaching saturation.

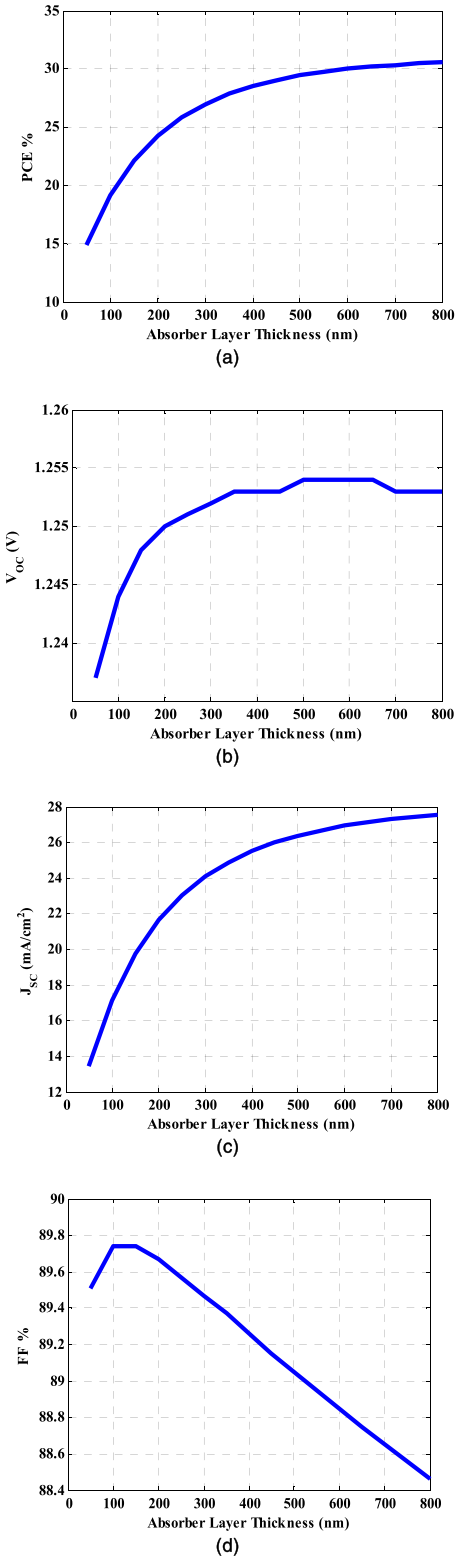

FIGURE 4. Characteristics of Perovskite ($MAPbI_{3-x}Cl_x$) with absorber thickness (T is 300 K, AM 1.5; electron and hole thermal velocities of 10^7 (cm/s)): (a) *PCE*, (b) V_{OC}, (c) J_{SC}, and (d) *FF*.

C. CIGS SUBCELL

Figure 5 presents the CIGS subcell's simulated J/V curve; the other used simulation conditions are the same as those

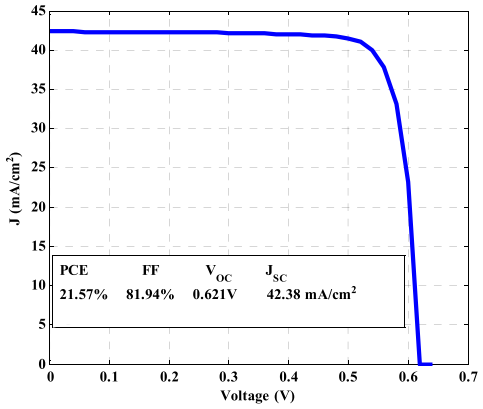

FIGURE 5. J/V simulated curve of CIGS cell (T is 300 K, AM 1.5; electron and hole thermal velocities of 10^7 (cm/s)).

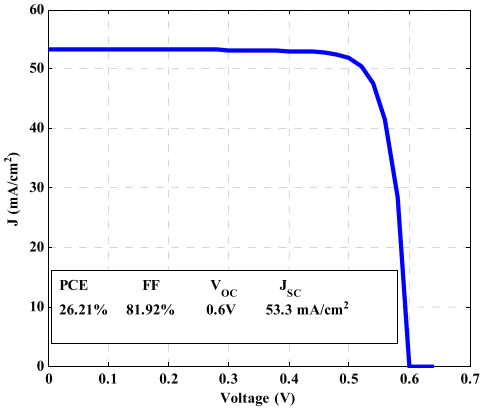

FIGURE 6. J/V simulated curve of GeTe cell (T is 300 K, AM 1.5; electron and hole thermal velocities of 10^7 (cm/s)).

used for the previous simulations. The simulated CIGS subcell exhibits a $PCE = 21.57$ % with $FF = 81.94\%$, $V_{OC} = 0.621$ V, and $J_{SC} = 42.38$ mA/cm^2.

D. GeTe SUBCELL

Figure 6 shows the simulated J/V curve of the GeTe subcell. The simulated GeTe subcell exhibits a $PCE = 26.21\%$ with $FF = 81.92$ %, $V_{OC} = 0.6$ V, and $J_{SC} = 53.3$ mA/cm^2.

The results show that GeTe is a promising material as it has a high short-circuit current density; which is the key to solve one of the main limitations of the two-terminal tandem solar cells; as the current density of the two-terminal tandem solar cells is limited by the lowest current of the subcells (mostly the bottom subcell). Therefore, GeTe is a better choice, especially for the bottom tandem subcells (low incident power spectrum). In addition to its electrical conductivity, the reason that GeTe has high current density is it has a low energy gap, which leads to the ability to absorb more of the incident spectrum.

E. TANDEM PEROVSKITE ($MAPbI_3$)/CIGS CELL

To perform the simulation of the optimized perovskite ($MAPbI_3$)/CIGS two-terminal tandem solar cell, the

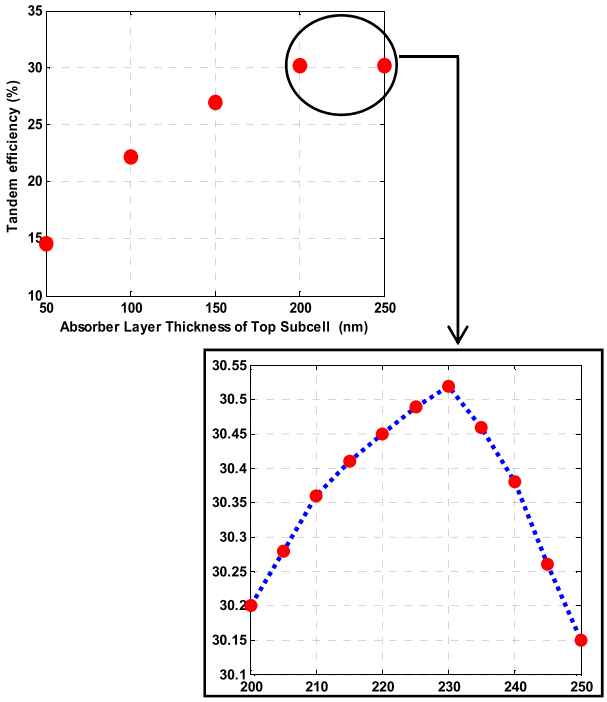

FIGURE 7. Perovskite ($MAPbI_3$)/ CIGS tandem cell efficiency with top subcell absorber layer thickness.

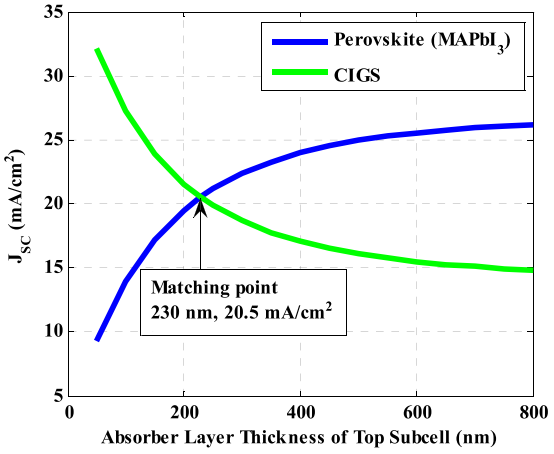

FIGURE 8. J_{SC} of perovskite ($MAPbI_3$) and CIGS subcells with top subcell absorber layer.

proposed numerical method was used, and the tandem output efficiency with top subcell absorber layer thickness is shown in Fig. 7. The results show the optimum (highest) tandem cell efficiency is 30.52% at top subcell absorber layer thickness 230 nm. Also the current density of both subcells was examined with varying the thickness of the absorbing layer of the top subcell and the results shows the matching point at perovskite thickness of 230 nm as shown in Fig. 8; the perovskite ($MAPbI_3$) subcell with this absorber layer thickness exhibits a $PCE = 20.58\%$ with $FF = 82.67$ %, $V_{OC} = 1.2143$V, and $J_{SC} = 20.5$ mA/cm^2.

Then the highest efficiency of the tandem cell is at the matching point of the current density of both subcells with a top subcell absorber layer thickness of 230 nm.

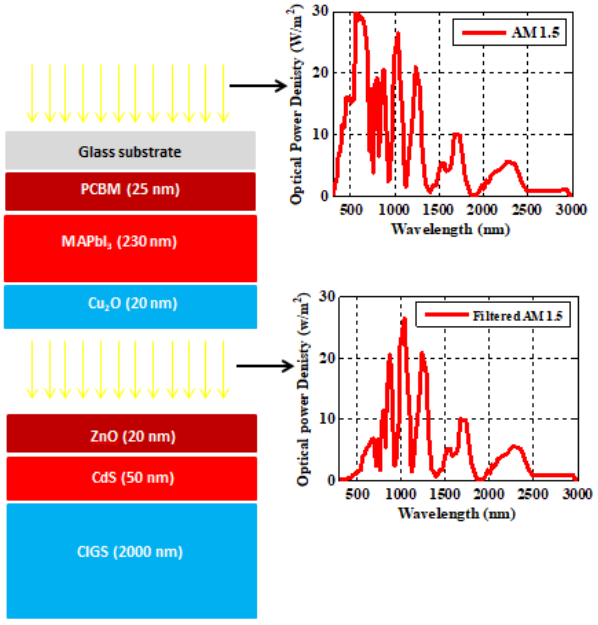

FIGURE 9. Perovskite ($MAPbI_3$)/CIGS tandem solar cell as AM1.5 and filtered AM 1.5 is illuminated on the subcells.

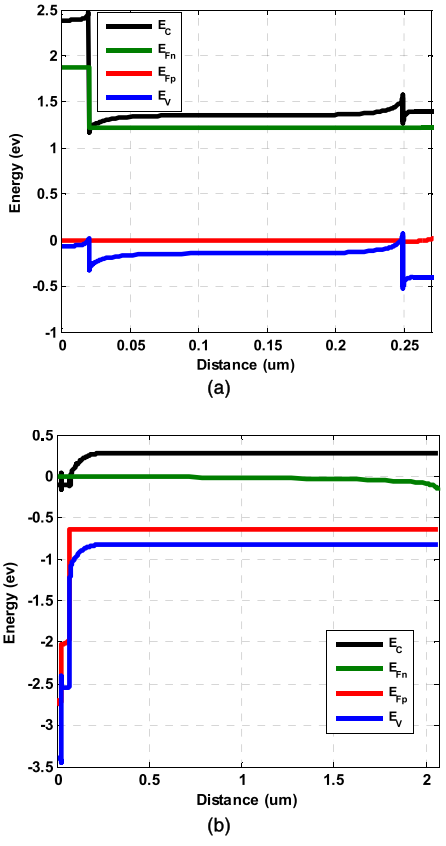

FIGURE 10. Band diagrams of Perovskite ($MAPbI_3$)/CIGS top and bottom subcells.

The structure of perovskite (MAPbI3)/ CIGS tandem cell with AM1.5 incident spectrum to the top subcell and filtered AM1.5 to the bottom subcell (after part of the spectrum is

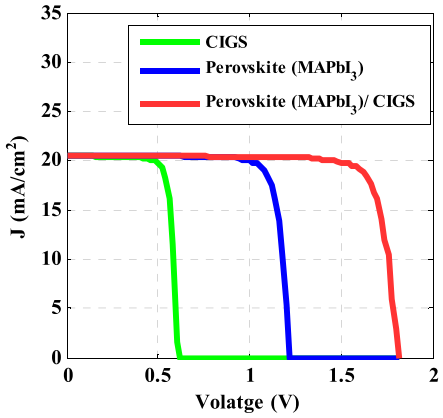

FIGURE 11. J/V curves of perovskite ($MAPbI_3$), CIGS subcells, and perovskite ($MAPbI_3$)/ CIGS tandem solar cell.

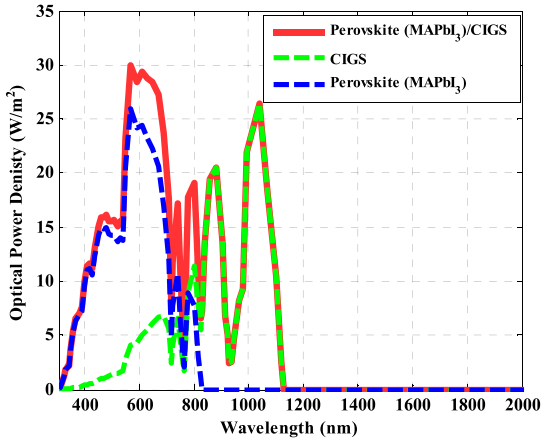

FIGURE 12. The absorbed spectrum of perovskite ($MAPbI_3$), CIGS subcells, and perovskite ($MAPbI_3$)/CIGS tandem cell.

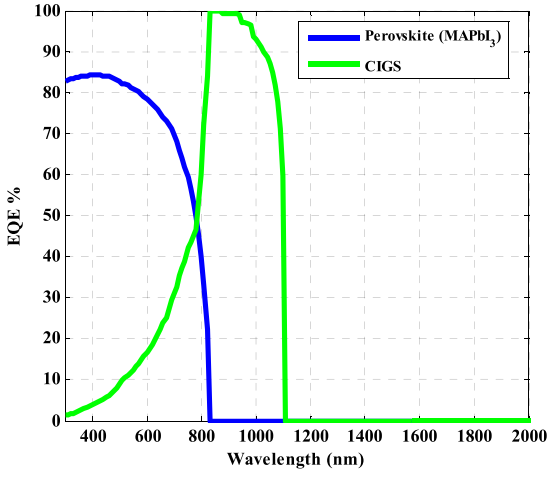

FIGURE 13. EQE of perovskite ($MAPbI_3$) and CIGS subcells.

absorbed by the top subcell) is shown in Fig. 9. The Figure shows that most of the AM 1.5 spectrum (up to 826 nm) is absorbed by the top subcell, and the rest of the spectrum is transmitted to the bottom subcell. The band diagrams of top and bottom subcells are shown in Fig. 10 a and b, respectively.

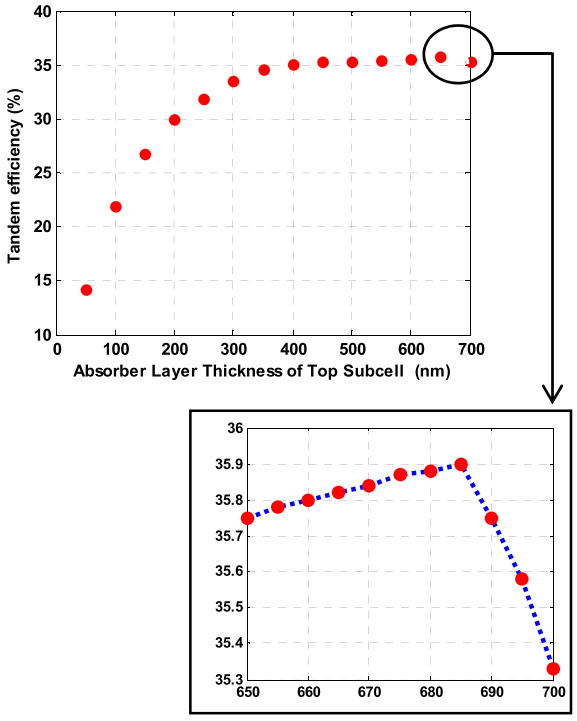

FIGURE 14. Perovskite ($MAPbI_3$)/GeTe tandem cell efficiency with top subcell absorber layer.

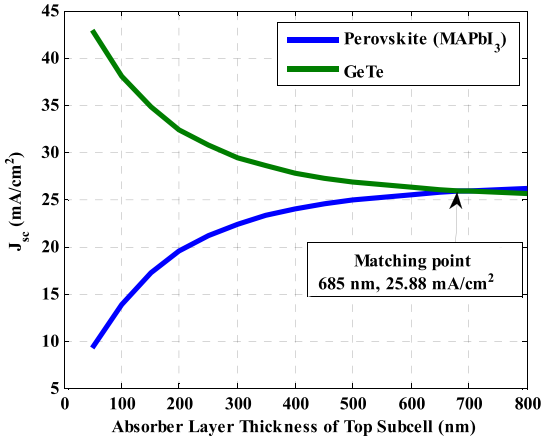

FIGURE 15. J_{SC} of the top perovskite ($MAPbI_3$) and bottom GeTe subcells with top subcell absorber layer.

J/V curves of perovskite ($MAPbI_3$), CIGS subcells and perovskite ($MAPbI_3$)/CIGS tandem solar cell are shown in Fig. 11. CIGS subcell with incident filtered AM 1. 5 spectrum exhibits a $PCE = 19.67\%$ with $FF = 81.19$ %, $V_{OC} = 0.603$ V, and $J_{SC} = 20.5$ mA/cm^2. Perovskite ($MAPbI_3$)/ CIGS tandem solar cell exhibits a $PCE = 30.52\%$ with $FF = 81.98$ %, $V_{OC} = 1.817$ V, and $J_{SC} = 20.5$ mA/cm^2. Figures 12 and 13 show the spectrum absorbed by perovskite ($MAPbI_3$), CIGS subcells and perovskite ($MAPbI_3$)/CIGS tandem solar cell, and the external quantum efficiency (EQE) of both subcells, respectively.

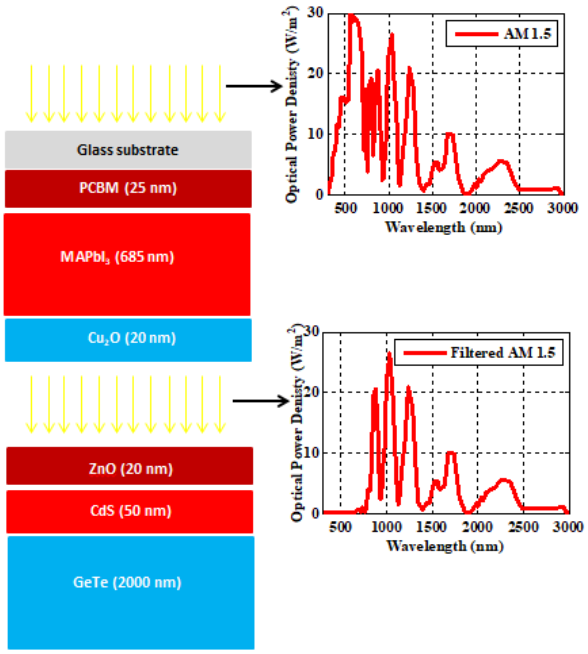

FIGURE 16. The perovskite ($MAPbI_3$)/GeTe tandem solar cell as AM1.5 and filtered AM 1.5 is illuminated on the subcells.

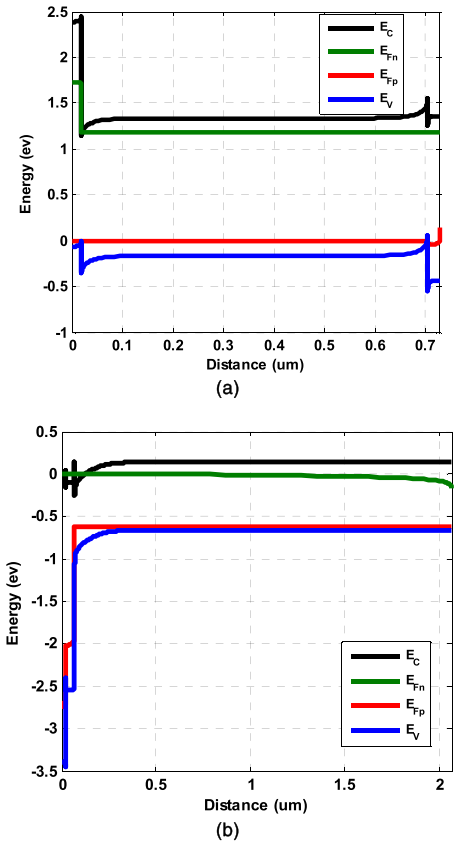

FIGURE 17. The band diagrams of Perovskite ($MAPbI_3$)/GeTe top and bottom subcells.

F. TANDEM PEROVSKITE ($MAPbI_3$)/GeTe CELL

In the perovskite ($MAPbI_3$)/ GeTe tandem solar cell, the bottom CIGS subcell of the previous tandem cell was replaced by a GeTe subcell with the same doping level and thickness.

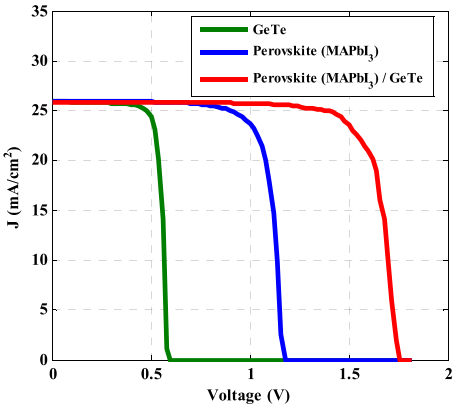

FIGURE 18. Fig.18. J/V curves of perovskite ($MAPbI_3$), GeTe subcells, and perovskite ($MAPbI_3$)/GeTe tandem solar cell.

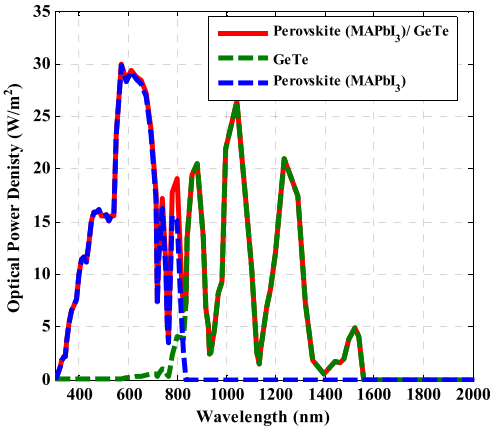

FIGURE 19. The absorbed spectrum of perovskite ($MAPbI_3$), GeTe subcells, and perovskite ($MAPbI_3$) GeTe tandem cell.

The thickness of the top subcell absorber layer (685 nm) is obtained using the proposed optimization numerical method, which results in 35.9% efficiency for the perovskite ($MAPbI_3$)/GeTe tandem cell, as shown in Fig. 14. The current densities of both subcells are examined with the top subcell thickness variation showing that the matching point is located at the optimum thickness obtained by the proposed algorithm, as shown in Fig. 15.

The perovskite ($MAPbI_3$) subcell with this absorber layer thickness exhibits a $PCE = 23.87\%$ with $FF = 78.71\%$, $V_{OC} = 1.1657$ V, and $J_{SC} = 25.88$ mA/cm^2. It is clear replacing the CIGS bottom subcell by the GeTe bottom subcell allows the top perovskite ($MAPbI_3$) to operate at a higher current density, which, in turn, improves the overall performance parameters of the tandem cell.

The structure of perovskite ($MAPbI_3$)/ GeTe tandem cell, with AM1.5 incident spectrum to the top subcell and filtered AM1.5 to the bottom subcell, is shown in Fig. 16.

The band diagrams of top and bottom subcells are shown in Fig. 17a, and b respectively. As expected, the spectrum absorbed by the top subcell (with 685 nm) is greater than

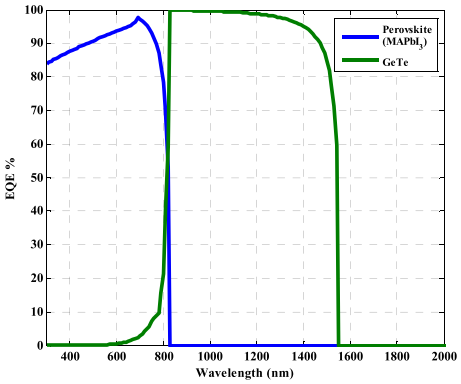

FIGURE 20. EQE of perovskite ($MAPbI_3$) and GeTe subcells.

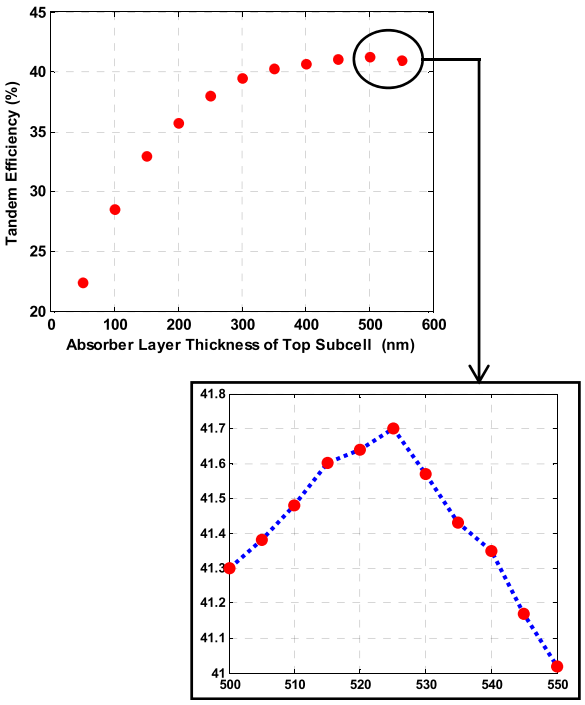

FIGURE 21. Perovskite ($MAPbI_{3-x}Cl_x$)/GeTe tandem cell efficiency with top subcell absorber layer thickness.

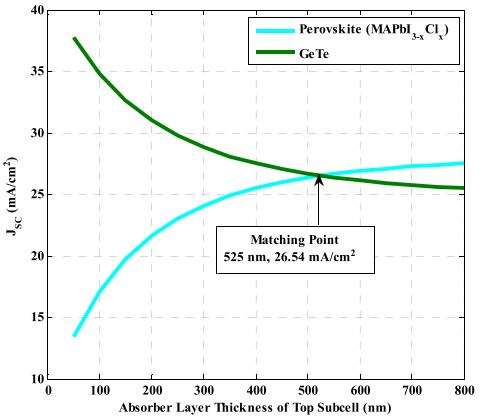

FIGURE 22. J_{SC} of the top perovskite ($MAPbI_{3-x}Cl_x$) and bottom GeTe subcells with top subcell absorber layer.

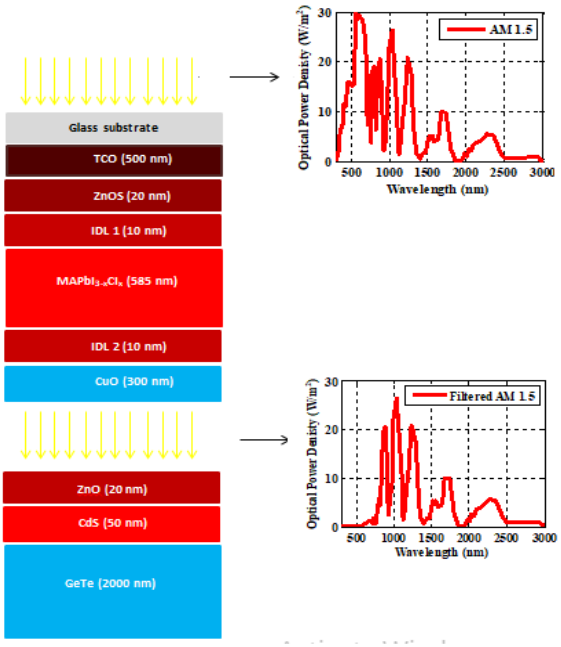

FIGURE 23. The perovskite ($MAPbI_{3-x}Cl_x$)/ GeTe tandem solar cell as AM1.5 and filtered AM 1.5 is illuminated on the top and bottom subcells.

that whose absorber layer thickness is about 230 nm. The new AM 1.5 filtered spectrum transmitted to the bottom subcell is lower than the previous tandem cell. However, because of the GeTe properties, the bottom subcell generates a higher current density of about 25.90 mA/cm^2, which almost matches the top subcell current density.

J/V curves of perovskite ($MAPbI_3$), GeTe subcells and perovskite ($MAPbI_3$)/ GeTe tandem solar cell are shown in Fig. 18. GeTe subcell with incident filtered AM 1. 5 spectrum exhibits a $PCE = 29.79\%$ with FF = 81.11 %, $V_{OC} = 0.581$ V, and $J_{SC} = 25.9$ mA/cm^2, perovskite ($MAPbI_3$)/ CIGS tandem solar cell exhibit a $PCE = 35.9\%$ with $FF = 79.40$ %, $V_{OC} = 1.747$ V, and $J_{SC} = 25.88$ mA/cm^2.

Figures 19 and 20 show the spectrum absorbed by perovskite ($MAPbI_3$), GeTe subcells and perovskite ($MAPbI_3$)/ GeTe tandem solar cell, and the external quantum efficiency (EQE) of both subcells, respectively.

G. TANDEM PEROVSKITE ($MAPbI_{3-x}Cl_x$)/GeTe CELL

The perovskite ($MAPbI_{3-x}Cl_x$)/GeTe tandem solar-cell is as the previous tandem cell with the top perovskite ($MAPbI_3$) subcell replaced by the optimized perovskite ($MAPbI_{3-x}Cl_x$) subcell [4]. The thickness of the top subcell absorber layer (525 nm) is obtained using the proposed optimization numerical method, resulting in a higher efficiency of 41.7% as shown in Fig. 21. At this thickness, both subcells' current densities are found to be almost the same as shown in Fig. 22.

As the perovskite ($MAPbI_{3-x}Cl_x$) has a higher open-circuit voltage relative to perovskite ($MAPbI_3$), the overall open-circuit voltage of the perovskite ($MAPbI_{3-x}Cl_x$)/GeTe tandem cell is greater than perovskite ($MAPbI_3$)/ GeTe tandem cell.

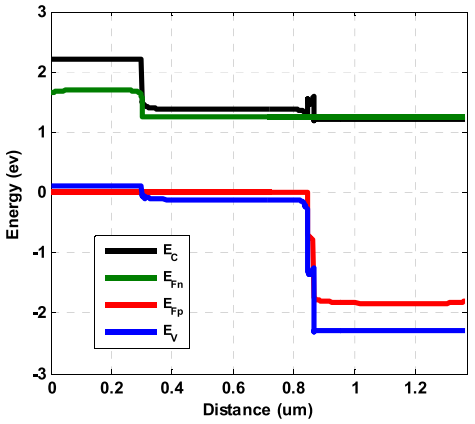

FIGURE 24. The band diagrams of Perovskite ($MAPbI_{3-x}Cl_x$) subcell.

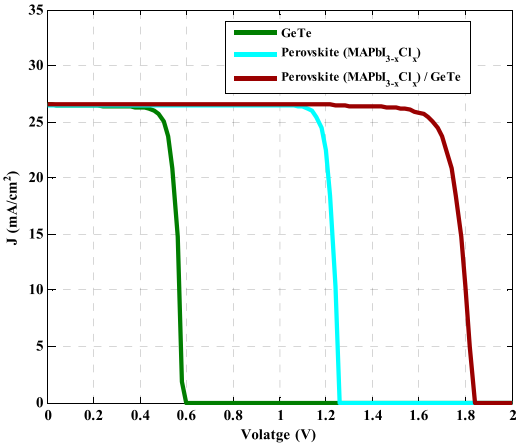

FIGURE 25. J/V curves of perovskite ($MAPbI_{3-x}Cl_x$), GeTe subcells, and perovskite ($MAPbI_{3-x}Cl_x$)/GeTe tandem solar cell.

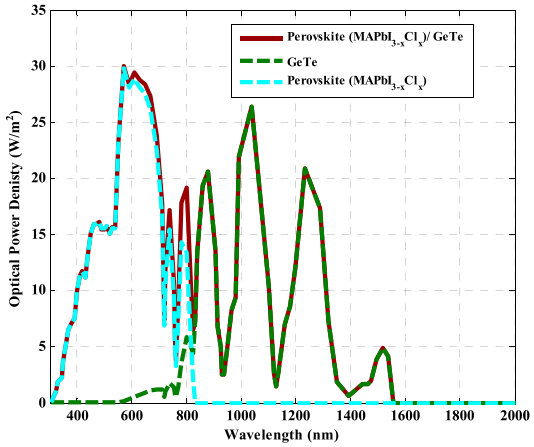

FIGURE 26. The absorbed spectrum of perovskite ($MAPbI_{3-x}Cl_x$), GeTe subcells and perovskite ($MAPbI_{3-x}Cl_x$)/ GeTe tandem cell.

The perovskite ($MAPbI_{3-x}Cl_x$) subcell with this absorber layer thickness exhibits a $PCE = 29.61\%$ with $FF = 88.99\%$, $V_{OC} = 1.254$ V, and $J_{SC} = 26.54$ mA/cm^2. It is clear that replacing the perovskite ($MAPbI_3$) top subcell with the perovskite ($MAPbI_{3-x}Cl_x$) top subcell leads to a higher matching current density point and higher open-circuit

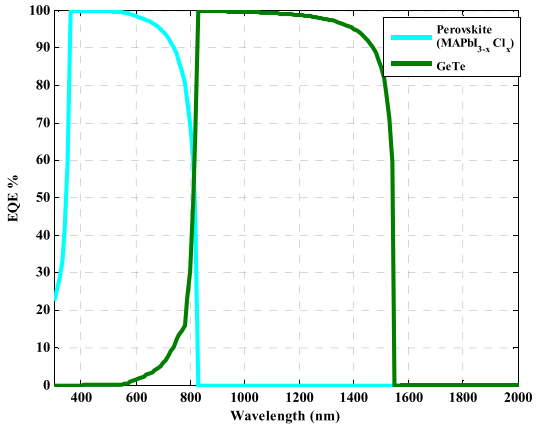

FIGURE 27. EQE of perovskite ($MAPbI_{3-x}Cl_x$) and GeTe subcells.

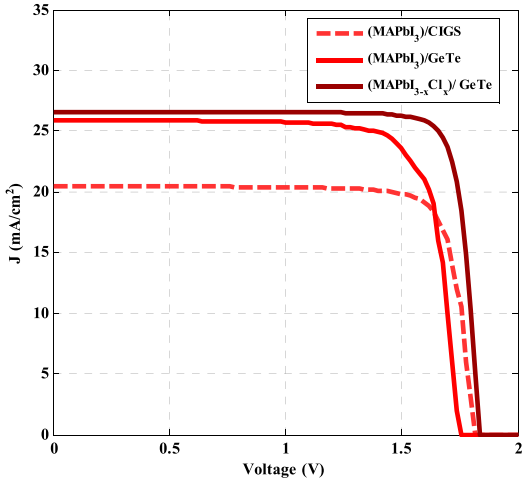

FIGURE 28. J/V curves of the three tandem cells $MAPbI_3$/CIGS, $MAPbI_3$/GeTe, and $MAPbI_{3-x}Cl_x$/GeTe with *PCE* 30.52%, 35.9%, and %41.73%, respectively.

voltage. As expected, this improves the overall performance parameters of the tandem perovskite ($MAPbI_{3-x}Cl_x$)/GeTe cell.

The structure of perovskite ($MAPbI_{3-x}Cl_x$)/GeTe tandem cell, with AM1.5 incident spectrum to the top subcell and filtered AM1.5 to the bottom subcell, is shown in Fig. 23. The spectrum absorbed by the top perovskite ($MAPbI_{3-x}Cl_x$) subcell is almost of the same wavelength (826 nm) as perovskite ($MAPbI_3$). The band diagram of top subcell is shown in Fig. 24.

The J/V curves of perovskite ($MAPbI_{3-x}Cl_x$), GeTe subcells and perovskite ($MAPbI_{3-x}Cl_x$)/GeTe tandem solar cell are shown in Fig. 25. GeTe subcell with incident filtered AM 1. 5 spectrum exhibits a PCE = 29.79% with $FF = 81.14$ %, $V_{OC} = 0.582$ V, and $J_{SC} = 26.57$ mA/cm^2. perovskite ($MAPbI_{3-x}Cl_x$)/GeTe tandem solar cell exhibits a $PCE = 41.7\%$ with $FF = 85.66$ %, $V_{OC} = 1.836$ V, and $J_{SC} = 26.54$ mA/cm^2. Figures 26 and 27 show the spectrum absorbed by perovskite ($MAPbI_{3-x}Cl_x$), GeTe subcells and perovskite ($MAPbI_{3-x}Cl_x$)/ GeTe tandem solar cell spectrum, and

TABLE 4. Performance parameters of three tandem cells.

Parameters	$MAPbI_3$/ CIGS	$MAPbI_3$/ GeTe	$MAPbI_{3-x}Cl_x$/ GeTe
η (%)	30.52	35.90	41.73
FF (%)	81.98	79.40	85.66
J_{SC} (mA/cm^2)	20.50	25.88	26.54
$V_{OC}(V)$	1.816	1.747	1.835

the external quantum efficiency (EQE) of both subcells, respectively.

H. PERFORMANCE COMPARISON OF THE THREE PROPOSED TANDEM CELLS

This section shows a comparison between the proposed three-tandem cells. First, the J/V curves of the three-tandem cells are given in Fig. 28, then a comparison between the performance parameters of the proposed three- tandem solar cells are given in Table 4.

The results show that replacing the CIGS bottom subcell in $MAPbI_3$/CIGS tandem cell by GeTe subcell leads to increasing the current density by almost 25%. This, in turn, improves the overall performance of the $MAPbI_3$/GeTe tandem cell, and the power conversion efficiency increases from 30.5% to 35.9%, but at the same time, the $MAPbI_3$/GeTe tandem cell has a lower open-circuit voltage than $MAPbI_3$/CIGS tandem cell by about 0.07 V.

This can be attributed to the fact that the short-circuit current density matching point using GeTe as bottom subcell occurs at a thicker absorber layer of top $MAPbI_3$ subcell, and as shown in Fig. 2(b) the open-circuit voltage of the $MAPbI_3$ top subcell decreases as the absorber layer thickness increases.

To increase both the voltage and current, and optimize the performance of the tandem cell, an optimized $MAPbI_{3-x}Cl_x$ cell [4] is used as a top subcell with GeTe bottom subcell. This, in turn, increases the cell's overall efficiency and makes it closer to the ideal cell.

The efficiency increases to be 41.73%, and FF becomes 85.66%. To the best of our knowledge, this cell has one of the highest performance's parameters.

IV. THE EFFECTS OF THE TEMPERATURE VARIATION ON THE PARAMETERS OF PERFORMANCE

Temperature change has a significant impact on the performance of solar cells, so this section is dedicated to the study of this effect on the main parameters of the proposed cells.

Figures 29 and 30 show the performance parameters of the subcells and tandem cells with temperatures varying from 260 K to 360 K, respectively. The temperature variation effect is examined by changing the temperature by step 5K on SCAPS-1D simulator.

The results show that increasing the temperature decreases the PCE of subcells and tandem cells in a linear manner. It is clear that both perovskite ($MAPbI_3$ and $MAPbI_{3-x}Cl_x$) subcells are more immune to the temperature variation than CIGS and GeTe subcells.

The degradation of tandem cell efficiency is dominated by the effect of the bottom subcell, which is more affected by the change in temperature.

The open-circuit voltage and fill factor decrease with temperature; $MAPbI_{3-x}Cl_x$ and GeTe subcells are more immune to temperature variations than $MAPbI_3$ and CIGS subcells, especially at high temperatures. The short-circuit current density of $MAPbI_{3-x}Cl_x$ and GeTe subcells have higher immunity to temperature variations than $MAPbI_3$ and CIGS subcells. This enables the tandem cell $MAPbI_{3-x}Cl_x$/GeTe to have almost the best performance parameters relative to the other proposed tandem cells.

V. COMPARISON WITH THE RECENTLY REPORTED RESULTS

This section is dedicated to comparing the results of the recently published tandem solar cells and the results of this research; this comparison focuses on the tandem cell

TABLE 5. Comparison of the recently published results with the proposed tandem cells.

PCE (η) %	*FF %*	*J_{SC} (mA/cm^2)*	*V_{OC} (V)*	*The material of Top/Bottom subcells*	*Ref. - Year*
21.4	79.9	15.8	1.692	$MAPbI_3$/SHJ	[37] - 2016
22.8	77.5	16.8	1.751	$Cs_{0.19}\,FA_{0.81}PbI_3$ /SHJ	[38] - 2017
22.8	73.8	17.6	1.75	$Cs_{0.07}Rb_{0.03}FA_{0.765}\,MA_{0.135}\,PbI_{2.55}\,Br_{0.45}$ /Si	[39] - 2017
23.6	79	18.1	1.65	$Cs_{0.17}\,FA_{0.83}\,Pb(Br_{0.17}I_{0.83})_3$ /SHJ	[40] - 2017
25	77	18.4	1.77	$FA_{0.75}\,Cs_{0.25}Pb(I_{0.8}Br_{0.2})_3$/Si	[41] - 2018
25.2	73.1	19.5	1.788	$Cs_xFA_{1-x}Pb(I,Br)_3$/textured Si	[42] - 2018
25.4	79.4	17.8	1.8	$Cs_{0.15}\,(FA_{0.83}MA_{0.17})_{0.85}\,Pb(I_{0.8}Br_{0.2})_3$/Si	[43] - 2018
25.5	78.5	18.5	1.76	$Cs_{0.05}\,(MA_{0.17}FA_{0.83})Pb_{1.1}(I_{0.83}\,Br_{0.17})_3$ /Si	[44] - 2018
28	78.7	19.75	1.8	Perovskite/Si (monolithic)	[45] - 2018
30.2	68.9	22.4	1.94	Se/CZTSSe	[46] - 2019
30.5	**81.9**	**20.49**	**1.81**	***$MAPbI_3$/CIGS***	***This work***
31.1	88	17.04	2.07	GaInP/Si	[47] - 2020
33.3	83.5	12.7	3.127	Triple-junction ($Ga_{0.51}\,In_{0.49}$ P/GaAs/Si)	[48] - 2018
35.9	87.5	13.6	2.52	Triple-junction (GaInP/GaAs/Si)	[49] - 2017
35.9	**79.40**	**25.88**	**1.747**	***$MAPbI_3$/GeTe***	***This work***
39.2	83.5	8.457	5.549	Six junction (monolithic)	[50] - 2017
41.73	**85.66**	**26.54**	**1.835**	***$MAPbI_{3-x}Cl_x$/ GeTe***	***This work***

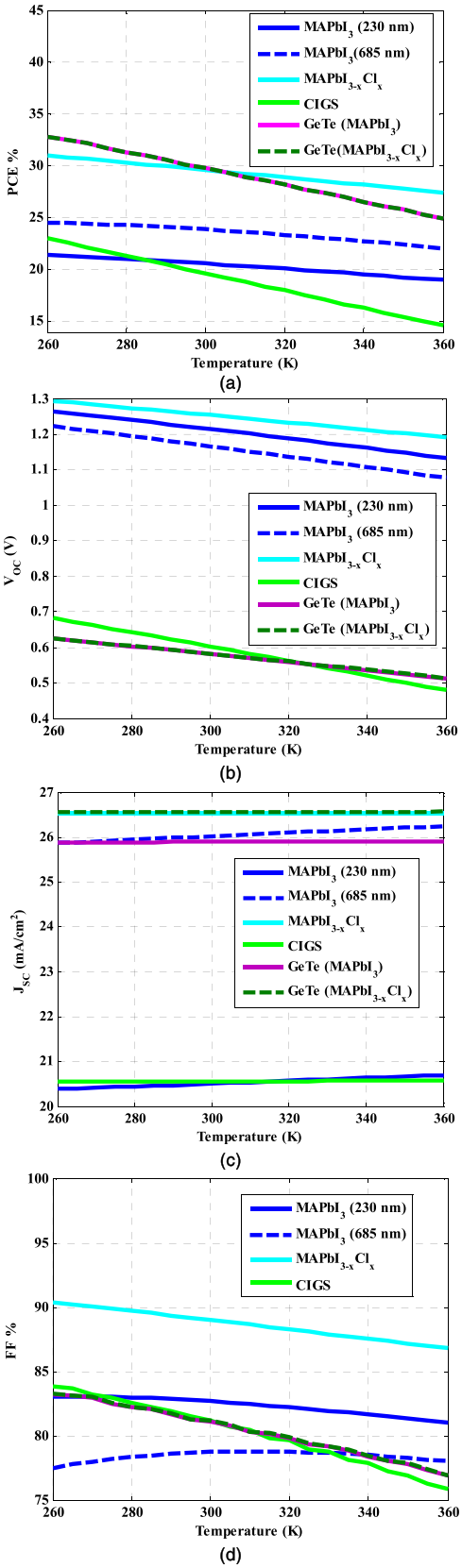

FIGURE 29. Performance of subcells with temperature: (a) *PCE*, (b) V_{OC}, (c) J_{SC}, and (d) *FF*.

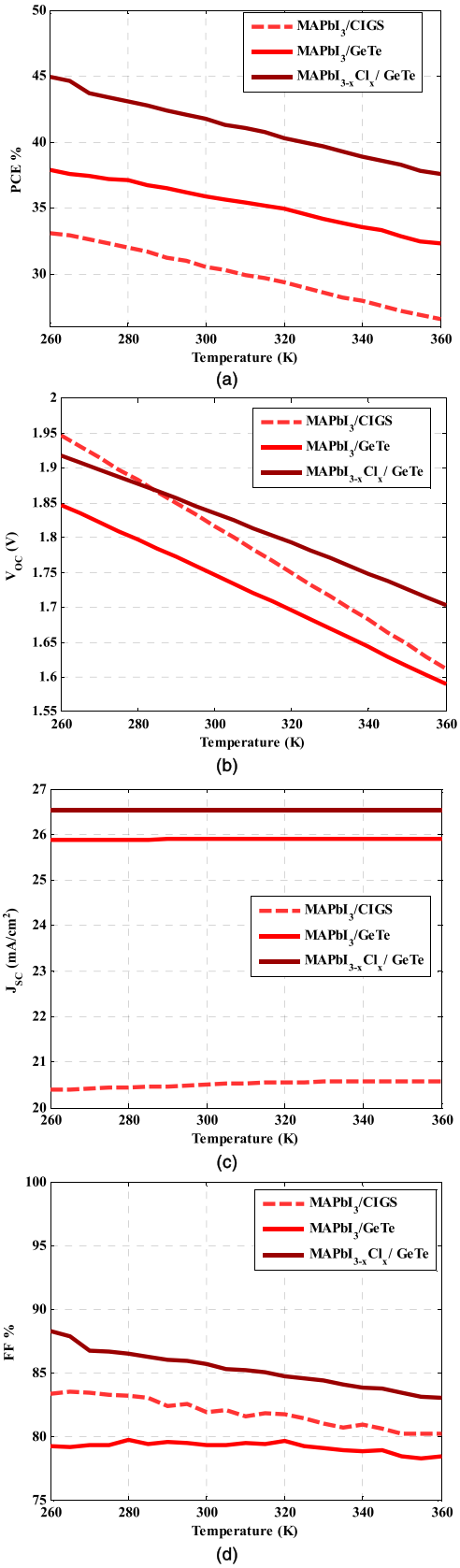

FIGURE 30. Performance of tandem cells with temperature: (a) *PCE*, (b) V_{OC}, (c) J_{SC}, and (d) *FF*.

main parameters of performance as listed in Table 5. It is noticed that the efficiency of the tandem solar cells is doubled in the last few years, and the new proposed tandem cells ($MAPbI_3$/CIGS, $MAPbI_3$/GeTe, and $MAPbI_{3-x}Cl_x$/GeTe) have high *PCE* relative to the other double junction two-terminal tandem cells. The triple (and more) junction solar cell shows high performance, but it is more complicated with a higher cost.The proposed $MAPbI_3$/GeTe, and $MAPbI_{3-x}Cl_x$/GeTe tandem cells have one of the highest *PCEs*, and best performance parameters for two-terminal double junction tandem cells, which is comparable to those of the conventional and the complicated (triple-junction and more) one. Up to our knowledge, this work reports one of the highest power conversion efficiency in recent years for two-junction tandem cells using incident spectrum AM 1.5.

VI. CONCLUSION

Along the road to manufacture solar cells with high power-conversion efficiency, multi-junction solar cells show a better choice as they can absorb a broader spectrum than single-junction solar cells. Increasing the number of junctions enhances the ability to absorb a wide spectrum and have a higher power-conversion efficiency. Still, at the same time, this increases the complexity and the cost of the cell. Only two-junction solar cells are used in this work and results in high efficiency. This is achieved by solving one of the main problems facing the two-terminal tandem solar cells, as the subcell with a lower current (almost the bottom) forces the tandem cell to operate at its current density. As the GeTe is used as an absorber in the bottom subcell, this shows a high current-density for the bottom subcells and allows the tandem cell to operate at a higher current, and this, in turn, increases the overall tandem cell performance. Also, a modified algorithm is proposed for optimizing the thickness of the top subcell layer. The simulations of the proposed tandem cell of $MAPbI_3$/CIGS show an efficiency of 30.5%; then, GeTe is used as a bottom subcell to replace the CIGS (with the same doping and thickness), which increased the efficiency to 35.9%. Replacing the $MAPbI_3$ top subcell by $MAPbI_{3-x}Cl_x$ shows a higher efficiency of 41.73%; which is one of the highest power-conversion efficiencies reported for tandem cells to the best of our knowledge. All the proposed cells have the advantages of using only two junctions, which greatly impact reducing the complexity and cost of solar cells.

REFERENCES

[1] N. T. Raj, S. Iniyan, and R. Goic, "A review of renewable energy based cogeneration technologies," *Renew. Sustain. Energy Rev.*, vol. 15, no. 8, pp. 3640–3648, 2011.

[2] K. Yoshikawa, H. Kawasaki, W. Yoshida, T. Irie, K. Konishi, K. Nakano, T. Uto, D. Adachi, M. Kanematsu, H. Uzu, and K. Yamamoto, "Silicon heterojunction solar cell with interdigitated back contacts for a photoconversion efficiency over 26%," *Nature Energy*, vol. 2, no. 5, 2017, Art. no. 17032.

[3] K. Sobayel, M. Shahinuzzaman, N. Amin, M. R. Karim, M. A. Dar, R. Gul, M. A. Alghoul, K. Sopian, A. K. M. Hasan, and M. Akhtaruzzaman, "Efficiency enhancement of CIGS solar cell by WS_2 as window layer through numerical modelling tool," *Sol. Energy*, vol. 207, pp. 479–485, Sep. 2020.

[4] M. M. Salah, M. Abouelatta, A. Shaker, K. M. Hassan, and A. Saeed, "A comprehensive simulation study of hybrid halide perovskite solar cell with copper oxide as HTM," *Semicond. Sci. Technol.*, vol. 34, no. 11, Nov. 2019, Art. no. 115009.

[5] R. Yasodharan, A. P. Senthilkumar, P. Mohankumar, J. Ajayan, and R. Sivabalakrishnan, "Investigation and influence of layer composition of tandem perovskite solar cells for applications in future renewable and sustainable energy," *Optik*, vol. 212, Jun. 2020, Art. no. 164723.

[6] M. Burgelman, K. Decock, S. Khelifi, and A. Abass, "Advanced electrical simulation of thin film solar cells," *Thin Solid Films*, vol. 535, pp. 296–301, May 2013.

[7] M. Mousa, M. M. Salah, F. Z. Amer, A. Saeed, and R. I. Mubarak, "High efficiency tandem perovskite/CIGS solar cell," in *Proc. 2nd Int. Conf. Smart Power Internet Energy Syst. (SPIES)*, Sep. 2020, pp. 224–227.

[8] K. Kim, J. Gwak, S. K. Ahn, Y.-J. Eo, J. H. Park, J.-S. Cho, M. G. Kang, H.-E. Song, and J. H. Yun, "Simulations of chalcopyrite/c-Si tandem cells using SCAPS-1D," *Sol. Energy*, vol. 145, pp. 52–58, Mar. 2017.

[9] K. Kim, J. S. Yoo, S. K. Ahn, Y.-J. Eo, J.-S. Cho, J. Gwak, and J. H. Yun, "Performance prediction of chalcopyrite-based dual-junction tandem solar cells," *Sol. Energy*, vol. 155, pp. 167–177, Oct. 2017.

[10] G. K. Gupta and A. Dixit, "Theoretical studies of single and tandem $Cu_2ZnSn(S/Se)_4$ junction solar cells for enhanced efficiency," *Opt. Mater.*, vol. 82, pp. 11–20, Aug. 2018.

[11] M. M. Lunardia, J. P. Alvarez-Gaitanb, J. I. Bilbaoa, and R. Corkisha, "Life cycle assessment of solar photovoltaics and their end-of-life," *IjoLCAS*, vol. 2, no. 2, 2018.

[12] J. Madan, Shivani, R. Pandey, and R. Sharma, "Device simulation of 17.3% efficient lead-free all-perovskite tandem solar cell," *Sol. Energy*, vol. 197, pp. 212–221, Feb. 2020.

[13] M. A. A. Noman, M. J. Abden, and M. A. Islam, "Germanium telluride absorber layer, a proposal for low illumination photovoltaic application using AMPS 1D," in *Proc. Int. Conf. Comput., Commun., Chem., Mater. Electron. Eng. (IC4ME2)*, Feb. 2018, pp. 1–5.

[14] U. Mandadapu, S. V. Vedanayakam, and K. Thyagarajan, "Simulation and analysis of lead based perovskite solar cell using SCAPS-1D," *Indian J. Sci. Technol.*, vol. 10, no. 11, pp. 65–72, 2017.

[15] K. P. Ganesan, N. Anandhan, V. Dharuman, P. Sami, R. Pannerselvam, and T. Marimuthu, "Electrochemically modified crystal orientation, surface morphology and optical properties using CTAB on Cu_2O thin films," *Results Phys.*, vol. 7, pp. 82–86, Jan. 2017.

[16] J.-Y. Jeng, Y.-F. Chiang, M.-H. Lee, S.-R. Peng, T.-F. Guo, P. Chen, and T.-C. Wen, "Methylammonium lead iodide perovskite/fullerene-based hybrid solar cells," *SPIE Newsroom*, vol. 10, Aug. 2013, Art. no. 005033.

[17] G. Xing, N. Mathews, S. Sun, S. S. Lim, Y. M. Lam, M. Gratzel, S. Mhaisalkar, and T. C. Sum, "Long-range balanced electron- and hole-transport lengths in organic-inorganic $CH_3NH_3PbI_3$," *Science*, vol. 342, no. 6156, pp. 344–347, Oct. 2013.

[18] L. Zhu, G. Shao, and J. Luo, "Numerical study of metal oxide heterojunction solar cells," *Semicond. Sci. Tech.*, vol. 26, Jun. 2011, Art. no. 085026.

[19] U. Mandadapu, "Simulation and analysis of lead based perovskite solar cell using SCAPS-1D," *Indian J. Sci. Technol.*, vol. 10, no. 1, pp. 1–8, Jan. 2017.

[20] G. Giorgi, J.-I. Fujisawa, H. Segawa, and K. Yamashita, "Small photocarrier effective masses featuring ambipolar transport in methylammonium lead iodide perovskite: A density functional analysis," *J. Phys. Chem. Lett.*, vol. 4, no. 24, pp. 4213–4216, Dec. 2013.

[21] K. Akaike, K. Kanai, H. Yoshida, J. Tsutsumi, T. Nishi, N. Sato, Y. Ouchi, and K. Seki, "Ultraviolet photoelectron spectroscopy and inverse photoemission spectroscopy of [6,6]-phenyl-C61-butyric acid methyl ester in gas and solid phases," *J. Appl. Phys.*, vol. 104, no. 2, Jul. 2008, Art. no. 023710.

[22] P. A. Korzhavyi and B. Johansson, *Literature Review on the Properties of Cuprous Oxide Cu_2O and the Process of Copper Oxidation*. Stockholm, Sweden: Swedish Nuclear Fuel and Waste Management Company, 2011.

[23] C. Wehrenfennig, G. E. Eperon, M. B. Johnston, H. J. Snaith, and L. M. Herz, "High charge carrier mobilities and lifetimes in organolead trihalide perovskites," *Adv. Mater.*, vol. 26, no. 10, pp. 1584–1589, Mar. 2014.

[24] Q. Zhou, D. Jiao, K. Fu, X. Wu, Y. Chen, J. Lu, and S.-E. Yang, "Two-dimensional device modeling of $CH_3NH_3PbI_3$ based planar heterojunction perovskite solar cells," *Sol. Energy*, vol. 123, pp. 51–56, Jan. 2016.

[25] H. Matsumura, A. Fujii, and T. Kitatani, "Properties of high-mobility Cu_2O films prepared by thermal oxidation of Cu at low temperatures," *Jpn. J. Appl. Phys.*, vol. 35, p. 5631, Nov. 1996.

[26] Y. S. Lee, J. Heo, M. T. Winkler, S. C. Siah, S. B. Kim, R. G. Gordon, and T. Buonassisi, "Nitrogen-doped cuprous oxide as a P-type hole-transporting layer in thin-film solar cells," *J. Mater. Chem. A*, vol. 1, no. 48, p. 15416, 2013.

[27] N. Kour, R. Mehra, and Chandni, "Efficient design of perovskite solar cell using mixed halide and copper oxide," *Chin. Phys. B*, vol. 27, no. 1, Jan. 2018, Art. no. 018801.

[28] J. Chae, Q. Dong, J. Huang, and A. Centrone, "Chloride incorporation process in $CH_3NH_3PbI_{3-x}Cl_x$ perovskites via nanoscale bandgap maps," *Nano Lett.*, vol. 15, no. 12, pp. 8114–8121, Dec. 2015.

[29] M. Gloeckler, "Device physics of Cu(In, Ga)Se_2 thin-film solar cells," Ph.D. dissertation, Dept. Phys., Colorado State Univ., Fort Collins, CO, USA, 2005.

[30] S. Bansal and P. Aryal, "Evaluation of new materials for electron and hole transport layers in perovskite-based solar cells through SCAPS-1D simulations," in *Proc. IEEE 43rd Photovoltaic Spec. Conf. (PVSC)*, Jun. 2016, pp. 1–4.

[31] S. I. Rahman, S. Faisal, S. Ahmed, and T. I. Dhrubo, "A comparative study on different HTMs in perovskite solar cell with ZnOS electron transport layer," in *Proc. IEEE Region Humanitarian Technol. Conf. (R10-HTC)*, Dec. 2017, pp. 546–550.

[32] T. Minemoto and M. Murata, "Theoretical analysis on effect of band offsets in perovskite solar cells," *Sol. Energy Mater. Sol. Cells*, vol. 133, pp. 8–14, Feb. 2015.

[33] M. M. Salah, K. M. Hassan, M. Abouelatta, and A. Shaker, "A comparative study of different ETMs in perovskite solar cell with inorganic copper iodide as HTM," *Optik*, vol. 178, pp. 958–963, Feb. 2019.

[34] A. O. Pudov, A. Kanevce, H. A. Al-Thani, J. R. Sites, and F. S. Hasoon, "Secondary barriers in CdS-$CuIn_{1-x}Ga_xSe_2$ solar cells," *J. Appl. Phys.*, vol. 97, no. 6, 2005, Art. no. 064901.

[35] S. Wagner, J. L. Shay, P. Migliorato, and H. M. Kasper, "$CuInSe_2$/CdS heterojunction photovoltaic detectors," *Appl. Phys. Lett.*, vol. 25, no. 8, pp. 434–435, Oct. 1974.

[36] R. I. Rabady and H. Manasreh, "Thicknesses optimization of two- and three-junction photovoltaic cells with matched currents and matched lattice constants," *Sol. Energy*, vol. 158, pp. 20–27, Dec. 2017.

[37] J. Werner, C. H. Weng, A. Walter, L. Fesquet, J. P. Seif, S. De Wolf, B. Niesen, and C. Ballif, "Efficient monolithic perovskite/silicon tandem solar cell with cell area> 1 cm^2," *J. Phys. Chem. Lett.*, vol. 7, no. 1, pp. 161–166, 2016.

[38] F. Sahli, B. A. Kamino, J. Werner, M. Bräuninger, B. Paviet-Salomon, L. Barraud, R. Monnard, J. P. Seif, A. Tomasi, Q. Jeangros, A. Hessler-Wyser, S. De Wolf, M. Despeisse, S. Nicolay, B. Niesen, and C. Ballif, "Improved optics in monolithic perovskite/silicon tandem solar cells with a nanocrystalline silicon recombination junction," *Adv. Energy Mater.*, vol. 8, no. 6, Feb. 2018, Art. no. 1701609.

[39] Y. Wu, D. Yan, J. Peng, Y. Wan, S. P. Phang, H. Shen, N. Wu, C. Barugkin, X. Fu, S. Surve, and D. Grant, "Monolithic perovskite/silicon-homojunction tandem solar cell with over 22% efficiency," *Energy Environ. Sci.*, vol. 10, no. 11, pp. 2472–2479, 2017.

[40] K. A. Bush, A. F. Palmstrom, J. Y. Zhengshan, M. Boccard, R. Cheacharoen, J. P. Mailoa, D. P. McMeekin, R. L. Hoye, C. D. Bailie, T. Leijtens, and I. M. Peters, "23.6%-efficient monolithic perovskite/silicon tandem solar cells with improved stability," *Nature Energy*, vol. 2, no. 4, pp. 1–7, 2017.

[41] K. A. Bush, S. Manzoor, K. Frohna, Z. J. Yu, J. A. Raiford, A. F. Palmstrom, H. P. Wang, R. Prasanna, S. F. Bent, Z. C. Holman, and M. D. McGehee, "Minimizing current and voltage losses to reach 25% efficient monolithic two-terminal perovskite-silicon tandem solar cells," *ACS Energy Lett.*, vol. 3, no. 9, pp. 2173–2180, 2018.

[42] F. Sahli, J. Werner, B. A. Kamino, M. Bräuninger, R. Monnard, B. Paviet-Salomon, L. Barraud, L. Ding, J. J. D. Leon, D. Sacchetto, and G. Cattaneo, "Fully textured monolithic perovskite/silicon tandem solar cells with 25.2% power conversion efficiency," *Nature Mater.*, vol. 17, no. 9, pp. 820–826, Sep. 2018.

[43] B. Chen, Z. Yu, K. Liu, X. Zheng, Y. Liu, J. Shi, D. Spronk, P. N. Rudd, Z. Holman, and J. Huang, "Grain engineering for perovskite/silicon monolithic tandem solar cells with efficiency of 25.4%," *Joule*, vol. 3, no. 1, pp. 177–190, 2019.

[44] M. Jošt, E. Köhnen, A. B. Morales-Vilches, B. Lipovšek, K. Jäger, B. Macco, A. Al-Ashouri, J. Krč, L. Korte, B. Rech, R. Schlatmann, M. Topič, B. Stannowski, and S. Albrecht, "Textured interfaces in monolithic perovskite/silicon tandem solar cells: Advanced light management for improved efficiency and energy yield," *Energy Environ. Sci.*, vol. 11, no. 12, pp. 3511–3523, Dec. 2018.

[45] Oxford PV. (2018). *Oxford PV Perovskite Solar Cell Achieves 28% Efficiency*. [Online]. Available: https://www.oxfordpv.com/news/oxford-pv-perovskite-solar-cell-achieves-28-efficiency

[46] H. Ferhati and F. Djeffal, "Exceeding 30% efficiency for an environment-friendly tandem solar cell based on Earth-abundant Se/CZTS materials," *Phys. E, Low-Dimensional Syst. Nanostruct.*, vol. 109, pp. 52–58, May 2019.

[47] M. Benaicha, L. Dehimi, F. Pezzimenti, and F. Bouzid, "Simulation analysis of a high efficiency GaInP/Si multijunction solar cell," *J. Semicond.*, vol. 41, no. 3, 2020, Art. no. 032701.

[48] R. Cariou, J. Benick, F. Feldmann, O. Höhn, H. Hauser, P. Beutel, N. Razek, M. Wimplinger, B. Bläsi, D. Lackner, and M. Hermle, "III-V-on-silicon solar cells reaching 33% photoconversion efficiency in two-terminal configuration," *Nature Energy*, vol. 3, no. 4, pp. 326–333, 2018.

[49] S. Essig, C. Allebé, T. Remo, J. F. Geisz, M. A. Steiner, K. Horowitz, L. Barraud, J. S. Ward, M. Schnabel, A. Descoeudres, and D. L. Young, "Raising the one-sun conversion efficiency of III-V/Si solar cells to 32.8% for two junctions and 35.9% for three junctions," *Nature Energy*, vol. 2, no. 9, 2017, Art. no. 17144.

[50] J. F. Geisz, M. A. Steiner, N. Jain, K. L. Schulte, R. M. France, W. E. Mcmahon, E. E. Perl, and D. J. Friedman, "Building a six-junction inverted metamorphic concentrator solar cell," *IEEE J. Photovolt.*, vol. 8, no. 2, pp. 626–632, Mar. 2018.

MOHAMED MOUSA received the bachelor's degree from Future University in Egypt, and the M.Sc. degree from Ain Shams University. He is currently pursuing the Ph.D. degree with the Electronics and Communications Engineering Department, Faculty of Engineering, Helwan University. He is also an Assistant Lecturer with the Electrical Engineering Department, Future University in Egypt.

FATHY Z. AMER received the B.Sc., M.S., and Ph.D. degrees in electronics and communications engineering from the Faculty of Engineering, Helwan University, in 1978, 1982, and 1990, respectively. He was with the Faculty of Engineering, Helwan University, as an Associate Professor in 2005 and a full-time Professor in 2009, in electronics and communications engineering, where he is currently a full-time Professor with the Department of Electronics and Communications Engineering. His current research interests include the areas of microelectronics, nanoelectronics, energy conversion, and fault diagnosis.

ROAA I. MUBARAK received the B.Sc., M.S., and Ph.D. degrees in electronics and communications engineering from the Faculty of Engineering, Helwan University, in 2001, 2004, and 2011, respectively. She is currently an Assistant Professor with the Department of Electronics and Communications Engineering with the Faculty of Engineering, Helwan University. Her current research interests include the areas of medical electronics, microelectronics, power conversion, and energy harvesting.

AHMED SAEED (Senior Member, IEEE) received the B.Sc. and M.Sc. degrees in electronics and communications engineering from Helwan University, and the Ph.D. degree from Ain Shams University. He was a Visiting Lecturer with the Faculty of Engineering, University of Porto, Portugal, and the University of Central Lancashire, U.K. He was a Postdoctoral Researcher with the Center of Nanoelectronics and Devices, The American University in Cairo. He is currently an Assistant Professor with the Electrical Engineering Department, Future University in Egypt. His current research interests include the areas of PV cells, energy conversion, signal integrity, and the IoT.